

# On the Sensitivity of a Hollow Sphere as a Multi-modal Resonant Gravitational Wave Detector

F. Dubath<sup>1</sup>, J. Extermann<sup>2</sup> and L. Gottardi<sup>3</sup>

<sup>1</sup> KITP, Kohn Hall, UCSB CA 93106, USA ‡

<sup>2</sup> GAP - Biophotonics, Université de Genève, 20 rue de l'Ecole de Médecine, CH-1211 Genève 4, Switzerland

<sup>3</sup>SRON National Institute for Space Research, Sorbonnelaan 2, 3584 CA Utrecht, Netherlands

E-mail: dubath@kitp.ucsb.edu

**Abstract.** We present a numerical analysis to simulate the response of a spherical resonant gravitational wave detector and to compute its sensitivity. Under the assumption of optimal filtering, we work out the sensitivity curve for a sphere first taking into account only a single transducer, and then using a coherent analysis of the whole set of transducers.

We use our model for computing the sensitivity and therefore compare different designs of spherical detectors. In particular we present the case of 1 meter radius bulk and hollow spheres equipped with transducers in TIGA configuration, and we explore the sensitivity of a hollow sphere as a multi-modal detector.

PACS numbers: 04.80.Nn, 95.55.Ym

Submitted to: *Class. Quantum Grav.*

‡ On leave from DPT, Université de Genève, Switzerland

## 1. Introduction

Direct detection of gravitational waves (GW) is still an unachieved goal. The sensitivity improvement of single detectors [1], to achieve the first detection, goes in parallel with the set-up of detector networks to perform real GW astronomy [2]. To that purpose, future GW detectors should be able to track GW arrival directions. Due to their symmetry, spherical resonant detectors are natural GW ‘telescope’ candidates. Moreover, such detectors are based on the same technology as resonant bars and can benefit of the decades of experience gained by the GW community with this kind of experimental setup.

A technical problem resides in the fact that big cryogenic resonant spheres with high quality factor are difficult to build and to cool down. One can partially bypass this problem using hollow spheres and we will eventually focus on this kind of resonator.

However, the main limitation when dealing with resonant detectors, is the small bandwidth compared with laser interferometers [3].

Great progress have been made using the tuning of the electrical mode [4] which allows to enlarge the bandwidth from few Hz to the order of 100 Hz around the resonance frequency. A possible way to further enlarge the bandwidth consists of monitoring other resonance frequencies of the antenna. In the case of a cylindrical detector this strategy is not convenient since the coupling of the  $n$ -th longitudinal mode to GW falls off as  $(2n + 1)^{-2}$ . However for a sphere the next mode quintuplet is tightly coupled to GW. Monitoring these modes is possible using many transducers, tuned at different frequencies. Here we explore this possibility and also consider a model of a double-mode transducer sensitive to two modes at different frequencies. We have to stress that both issues are experimental challenges but they can lead to great improvement for spherical detectors.

It is possible to enlarge the detector bandwidth by monitoring also the second quadrupolar mode. In this way one could for example study the radiation emitted by a binary system, consisting of either neutron stars or black holes, in the in-spiral phase and determines the chirp mass by measuring the time delay between excitations of the first and second quadrupole modes of an hollow sphere [5]. Used as a multi-modal detector even a *single* sphere is able to set limit on the stochastic GW background [7]. Furthermore, with an appropriate resizing of the sphere, the second quadrupolar modes can be shifted to the frequency region where existing small spherical detectors are sensitive. This would open the possibility of coincidence search between several spherical detectors and the DUAL detector [21], building in this way the base for a powerful omnidirectional gravitational wave observatory.

In order to be able to compare different GW detectors we need to work out the sensitivity with a “standard” approach and we decided to use the strain sensitivity. A first goal of this paper is to furnish a mathematical framework to describe all the internal noises of a given detector and its response to an excitation (as example to a GW burst). This is realized as a matrix model in the Fourier space. Using this model, we

set up numerical simulations and first compute the sensitivity of each single transducer attached to the sphere. We are fully aware that performing the data analysis in this way does not exploit all the capacity of the spherical geometry. However, this first computation is instructive and may be useful in order to calibrate a future experiment. We point out the fact that the noise coming from the other transducers will then be an important limitation to the sensitivity. A clever way to use a spherical detector is to perform the data analysis combining the signals from all the transducers. Such a strategy, which requires multidimensional matched filtering [17, 18, 13], exploits all the geometrical properties of the detector and therefore gives best sensitivity. This is the sensitivity to be compared with other existing computations [8].

The second part of this paper will be dedicated to the application of our model to “realistic” detectors having in mind the comparison of different possible spherical resonant GW detectors. We will focus on hollow spheres and in particular we explore the different way to realize a multi-modal detector. The possibilities we test are all technical challenges (dealing with 12 transducers, transducer inside the hollow sphere, double mode transducers) but we eventually show that there is no gain in working with transducer inside the sphere and that 6 double mode transducers may compete with 12 single transducers configurations only if they have a very peculiar design.

## 2. First part: the model

### 2.1. Description of spherical resonant GW detectors

*2.1.1. The modes of a sphere* The vibrational motion of a rigid body can be split into eigen-modes. For a sphere there are two families of vibrational eigen-modes: toroidal and spheroidal [10]. Each mode can be described as a forced damped harmonic oscillator, which means that the  $j$ -th mode § amplitude  $z_j$  satisfies in Fourier space the equation (see for example [6])

$$\left( \omega_{s,j}^2 - \omega^2 + i \frac{\omega \omega_{s,j}}{Q_{s,j}} \right) \tilde{z}_j(\omega) = \frac{1}{m_s} \tilde{F}_j(\omega) , \quad (1)$$

where  $m_s$  is the physical mass of the sphere,  $\omega_{s,j}$  is the  $j$ -th mode eigen-frequency,  $Q_{s,j}$  its quality factor and  $\tilde{F}_j(\omega)$  the Fourier component of the forcing. The forcing of the mode is due to a stochastic (Langevin) force and to external forces. The stochastic force corresponds to the thermal excitation of the sphere mode. Among the external forces we retain only the tidal forces induced by GW, and forces due to the coupling of the mode with the transducers.

We use the frequencies  $\omega_{s,j}$  as an input for our model. The computation of the  $\omega_{s,j}$  can be found in [11].

§ We use  $j$  to describe collectively all the numbers needed to specify the mode. For spheroidal modes  $j = \{n, l, m\}$  [6]. In the following we will work with a subset of the modes. In particular we will use only  $J$  spheroidal modes that we will label by  $j = 1, \dots, J$

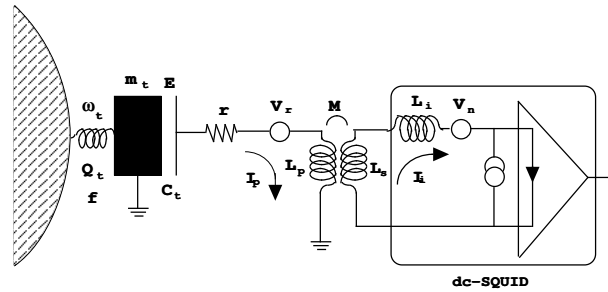


**Figure 1.** The transducer model.

*2.1.2. Transducer* To give a clear presentation of the noises and the sensitivity we need a full model for the transducer. We use capacitive transducers (Figure 1), based on the one employed on bar detector[1] and the spherical detector MiniGRAIL [12], composed by one resonator coupled to a dc-SQUID with input transformer, where the SQUID is described as a linear current amplifier [14]. However our formalism can be adapted for other kinds of transducer.

Each transducer (a mechanical resonator with its read-out) will be modelled by a set of  $p = 3$  coupled differential equations, driven by the specific intrinsic noises and its coupling to the sphere. In Fourier space each transducer and each read-out are described by the equation set

$$\begin{pmatrix} m_t (\omega_t^2 - \omega^2 + i\frac{\omega\omega_t}{Q_t}) & -iE/\omega & 0 \\ E & r + i(\omega L_p - \frac{1}{\omega C_t}) & -iM\omega \\ 0 & -iM\omega & i\omega(L_s + L_i) \end{pmatrix} \begin{pmatrix} \tilde{x} \\ \tilde{I}_p \\ \tilde{I}_i \end{pmatrix} = \begin{pmatrix} \tilde{f} \\ \tilde{V}_r \\ \tilde{V}_n \end{pmatrix} \quad (2)$$

where  $m_t$ ,  $\omega_t$ ,  $Q_t$  are the resonators mass, eigen-frequency and quality factor,  $E$  is the electric field in the capacitor  $C_t$  formed with the resonator,  $r$  the transformer resistance,  $L_i$ ,  $L_p$ ,  $L_s$  the inductances of the SQUID input coil, primary and secondary of the transformer, and  $M$  the mutual inductance of the transformer; see Figure 1.  $\tilde{x}$  is the transducers position [15],  $\tilde{I}_p$ ,  $\tilde{I}_i$  are the currents into the transformer and the SQUID, and  $\tilde{I}_i$  is the measured quantity. Finally,  $\tilde{V}_r$  and  $\tilde{V}_n$  are the voltages corresponding to the intrinsic noise and  $\tilde{f}$  is the sum of the thermal force and the forces due to the coupling to the spheres modes, which are described in Section 2.1.4.

In what follow, we will use a set of  $N$  transducers and therefore add an index  $k = 1, \dots, N$  to all the quantities describing the transducer.

*2.1.3. Double-mode transducer* Having in mind the possibility of building a multi-modal spherical resonant GW antenna we note that a simple way to achieve this goal is the use of multi-modal transducers. A multi-modal transducer has to be designed in order to be resonantly coupled to two distinct frequencies. As a model, one can think to a multi-modal resonator with different vibration frequencies, (each frequency tuned on one of the sphere resonance frequencies) and corresponding electronic read-out. The

resonator can be modelled as two oscillators located at the same point of the sphere.

In Figure 2, we show the schematic diagram of a capacitive double mode transducer composed of a resonator mechanically coupled to the two first spheroidal modes of the sphere and a single SQUID read-out. The two resonating mass schematically drawn in the figure should be considered fixed at the same point on the sphere surface. Such a transducer could be fabricated using, for example, a mushroom type resonator placed inside a ring-shaped membrane transducer or using the geometry suggested in [25]. By means of two electrically insulated electrodes and two super-conducting matching transformers, one is able to couple the signal from both the resonators to a single SQUID amplifier, simplifying greatly the detector read-out electronics and the cryostat wiring. To achieve an optimal impedance matching each electrical mode defined by the two LC circuits should be coupled to the two corresponding spheroidal modes. In this scheme a mixing may occur between the two modes. However we will show here that this will not significantly reduce the detector sensitivity.

The double-mode transducer is described by a set of  $p = 5$  equations: two for the mechanical modes, two for the transformer currents  $I_1, I_2$ , and one for the SQUID input current  $I_i$ :

$$\left( \omega_{t1}^2 - \omega^2 + i \frac{\omega \omega_{t1}}{Q_{t1}} \right) \tilde{x}_{t1} - i \frac{E_1}{\omega} \tilde{I}_1 = \tilde{f}_1 \quad (3)$$

$$\left( \omega_{t2}^2 - \omega^2 + i \frac{\omega \omega_{t2}}{Q_{t2}} \right) \tilde{x}_{t2} - i \frac{E_2}{\omega} \tilde{I}_2 = \tilde{f}_2 \quad (4)$$

$$E_1 \tilde{x}_{t1} + \left( r_1 + i \omega L_{1,p} - \frac{i}{\omega C_1} \right) \tilde{I}_1 - i \omega M_1 \tilde{I}_i = \tilde{V}_{1,r} \quad (5)$$

$$E_2 \tilde{x}_{t2} + \left( r_2 + i \omega L_{2,p} - \frac{i}{\omega C_2} \right) \tilde{I}_2 - i \omega M_2 \tilde{I}_i = \tilde{V}_{2,r} \quad (6)$$

$$i \omega (L_{1,s} + L_{2,s} + L_i) \tilde{I}_i - i \omega (M_1 \tilde{I}_1 + M_2 \tilde{I}_2) = \tilde{V}_n, \quad (7)$$

where  $E_i$ ,  $i = 1, 2$  is the electrical field in the  $i$ -th capacitors and  $\tilde{x}_{ti}$  the displacement of the two mechanical modes.

$$\begin{pmatrix} \left( \omega_{t1}^2 - \omega^2 + i \frac{\omega \omega_{t1}}{Q_{t1}} \right) & 0 & -i \frac{E_1}{\omega} & 0 & 0 \\ 0 & \left( \omega_{t2}^2 - \omega^2 + i \frac{\omega \omega_{t2}}{Q_{t2}} \right) & 0 & -i \frac{E_2}{\omega} & 0 \\ E_1 & 0 & r_1 + i \left( \omega L_{1,p} - \frac{1}{\omega C_1} \right) & 0 & -i M_1 \omega \\ 0 & E_2 & r_2 + i \left( \omega L_{2,p} - \frac{1}{\omega C_2} \right) & 0 & -i M_2 \omega \\ 0 & 0 & -i M_1 \omega & -i M_2 \omega & i \omega (L_{1,s} + L_{2,s} + L_i) \end{pmatrix} \times \begin{pmatrix} \tilde{x}_{t1} \\ \tilde{x}_{t2} \\ \tilde{I}_1 \\ \tilde{I}_2 \\ \tilde{I}_i \end{pmatrix} = \begin{pmatrix} \tilde{f}_1 \\ \tilde{f}_2 \\ \tilde{V}_{1,r} \\ \tilde{V}_{2,r} \\ \tilde{V}_n \end{pmatrix} \quad (8)$$

*2.1.4. Coupling transducers to the modes of the sphere* Since none of the state-of-the-art transducers are able to couple efficiently to tangential motion, we will restrict ourself

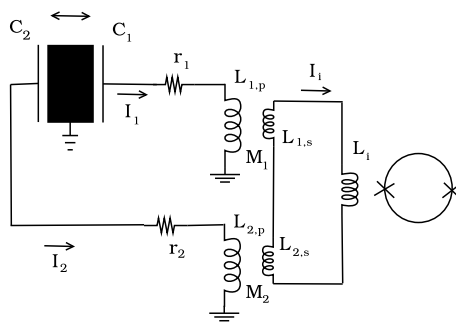


**Figure 2.** The double transducer model.

to transducers only sensitive to radial motion of the sphere, and consequently we will neglect the coupling to toroidal modes [10].

We call  $(\theta_k, \phi_k)$  the location of the  $k$ -th transducer. At this position on the sphere surface, the  $j = \{n, l, m\}$ -th spheroidal mode induces a radial displacement described

$$\alpha_{nl}(R_s)Y_{lm}(\theta_k, \phi_k) \equiv \alpha_j B_{jk} \quad (9)$$

where  $\alpha_j \equiv \alpha_{nl}(R_s)$  is the radial eigen-function evaluated at the sphere surface, and  $Y_{lm}$  is a spherical harmonic. This equation defines the pattern matrix  $B_{jk}$ . Using this matrix we obtain the equation of motion ([6], [13]). The coupling between the sphere modes and the transducers is then given (in the Fourier space) by

$$\tilde{F}_j = \tilde{F}_j^{\text{noise+GW}} + \sum_k \alpha_j B_{jk} \left( \left( \omega_{t,k}^2 + i \frac{\omega \omega_{t,k}}{Q_{t,k}} \right) m_{t,k} \tilde{x}_k - \tilde{f}_k^{\text{noise}} \right) \quad (10)$$

$$\tilde{f}_k = \tilde{f}_k^{\text{noise}} + m_{t,k} \omega^2 \sum_j B_{jk} \alpha_j \tilde{z}_j. \quad (11)$$

We obtain a set of  $(J + pN)$  coupled equations, with  $J$  the number of modes taken into account that we discuss bellow,  $N$  the number of transducers and  $p$  the number of equations need to describe a single transducer.

It is important to note that generally a transducer is coupled with a subset of the five sphere modes and therefore the presence of transducers provides an indirect coupling between the different modes. Reciprocally, different transducers are coupled through the sphere modes. Therefore, the total noise spectrum of a given transducer has a contribution from the intrinsic noises of the other transducers.

We are principally interested in the quadrupolar ( $\ell = 2$ ) spheroidal mode family. The lowest quadrupolar multiplet ( $n = 1, \ell = 2$ ) has the advantage to contain the 5 spheroidal modes with the lowest resonance frequency [11]. When we are only interested in those modes we can reduce the sphere vibration to these 5 modes and neglect the effect of the modes at higher frequency. When we describe a multi-modal detector, we are also interested in the second quadrupolar multiplet ( $n = 2, \ell = 2$ ) at about 2 times the fundamental mode resonance. We note that other modes, not coupled to GW, ( $n = 1, \ell = 0, 1, 3, 4$ ) have their resonance frequency between the ones of the first and second quadrupolar multiplet [11]. These modes induce additional thermal noise sources

and have to be included when calculating the sensitivity of a multi-modal resonator, like previously shown in [22].

*2.1.5. Bulk sphere model* The remaining of the computation is easier to follow if applied to a concrete example. For this purpose, we present a simple model with only the spheroidal quadrupole modes of the sphere ( $J = 5$ ,  $l = 2$ ), and with  $N = 6$  capacitive transducers placed in the TIGA configuration || [6]. Note that we can write the system of  $(J + pN)$  equations in the same form independently of the number of modes and transducers. We also use this example in order to set the notations.

Collecting the equations (1,2,9,10) and (11) we obtain a description of the entire detector as

$$\underbrace{\begin{pmatrix} \mathbf{S} & \mathbf{C}_1 & 0 \\ \mathbf{C}_2 & & \\ 0 & & \mathbf{T} \end{pmatrix}}_{\mathbf{Z}} \begin{pmatrix} \tilde{\mathbf{z}} \\ \tilde{\mathbf{q}} \\ \tilde{\mathbf{I}}_p \\ \tilde{\mathbf{I}}_i \end{pmatrix} = \underbrace{\begin{pmatrix} \mathbb{1}_5 & -\alpha\mathbf{B} & 0 & 0 \\ 0 & \mathbb{1}_6 & 0 & 0 \\ 0 & 0 & \mathbb{1}_6 & 0 \\ 0 & 0 & 0 & \mathbb{1}_6 \end{pmatrix}}_{\mathbf{A}} \begin{pmatrix} \tilde{\mathbf{F}}^{\text{noise+GW}} \\ \tilde{\mathbf{f}}^{\text{noise}} \\ \tilde{\mathbf{V}}_r \\ \tilde{\mathbf{V}}_n \end{pmatrix} \quad (12)$$

where  $\tilde{\mathbf{z}} = \begin{pmatrix} \tilde{z}_1 \\ \vdots \\ \tilde{z}_5 \end{pmatrix}$ ,  $\tilde{\mathbf{q}} = \begin{pmatrix} \tilde{x}_1 \\ \vdots \\ \tilde{x}_6 \end{pmatrix}$ , and so on for the other variables.

$\mathbf{S}$  is a  $5 \times 5$  diagonal sub-matrix given by the left hand side (LHS) of (1),  $\mathbf{T}$  is a  $3 \cdot 6 \times 3 \cdot 6$  sub-matrix with structure given by the LHS of (2) (each number in (2) is now a  $6 \times 6$  diagonal matrix). The matrices  $\mathbf{C}_1$  and  $\mathbf{C}_2$  are  $5 \times 6$  (resp.  $6 \times 5$ ) sub-matrix read out of (10,11) ¶ which describe the mechanical coupling between the spheroidal modes and the transducer modes and are given by

$$\mathbf{C}_1 = -\alpha\mathbf{B}\text{Diag}\left(m_{t,k}(\omega_{t,k}^2 + i\frac{\omega\omega_{t,k}}{Q_{t,k}})\right) \quad (13)$$

$$\mathbf{C}_2 = -\alpha\omega^2\text{Diag}(m_{t,k})\mathbf{B}^T. \quad (14)$$

## 2.2. Detector noise description

Starting from equation (12), knowing the forces and the voltage acting on the detector allows us to compute the sphere modes  $\tilde{\mathbf{z}}$ , the displacement  $\tilde{\mathbf{q}}$  of the transducer, and the currents  $\tilde{\mathbf{I}}_p$  and  $\tilde{\mathbf{I}}_i$ . To do that we invert the  $\mathbf{Z}$  matrix and rewrite (12) as

$$\begin{pmatrix} \tilde{\mathbf{z}} \\ \tilde{\mathbf{q}} \\ \tilde{\mathbf{I}}_p \\ \tilde{\mathbf{I}}_i \end{pmatrix} = \underbrace{\mathbf{Z}^{-1}}_{\mathbf{G}} \begin{pmatrix} \tilde{\mathbf{F}}^{\text{noise+GW}} \\ \tilde{\mathbf{f}}^{\text{noise}} \\ \tilde{\mathbf{V}}_r \\ \tilde{\mathbf{V}}_n \end{pmatrix} \quad (15)$$

|| The precise location of the transducer changes the  $B$  matrix causing to loose the TIGA configuration. However this do not change the following analysis

¶ As we have only modes with  $l = 2$ , all the  $\alpha_j$  are equal. Therefore, we drop the indices.

Mode amplitudes, transducer displacement and transformer currents are not directly measured and we are therefore interested only in the  $N$  last lines of  $\mathbf{G}$ , which give the proportionality coefficients between forces (and voltages) and SQUID input currents  $\tilde{\mathbf{I}}_i$ .

We now describe the different noise contributions.

*2.2.1. Noise description* We restrict ourself to the case where the disturbances  $\mathbf{F}^{\text{noise}}$ ,  $\mathbf{f}^{\text{noise}}$  and  $\mathbf{V}_r$  are only due to thermal excitations. In this case we can only access statistical property of these forces that is:

$$\langle F(t) \rangle = 0 \quad \langle V(t) \rangle = 0 , \quad (16)$$

$$\langle F(t)F(t') \rangle = A_0\delta(t - t') \quad \langle V(t)V(t') \rangle = A_0^e\delta(t - t') . \quad (17)$$

Furthermore one can compute [16] that the coefficient  $A_0$  takes the form

$$A_0 = 2k_B T m / Q \quad A_0^e = 2k_B T r . \quad (18)$$

where  $k_B$  is the Boltzmann constant,  $T$  is the thermodynamic temperature of the detector, and  $r$  the transformer resistance.

Using the definition of the single-sided spectral density of the force which is obtained through the autocorrelation

$$\langle F(t)F(t') \rangle = \frac{1}{2} \int_0^\infty \frac{d\omega}{2\pi} S_F(\omega) e^{-i\omega(t-t')} , \quad (19)$$

we obtain

$$\mathbf{S}_{F,j} = 4m_s \omega_{s,j} \frac{k_B T}{Q_{s,j}} \quad (20)$$

$$\mathbf{S}_{f,k} = 4m_{t,k} \omega_{t,k} \frac{k_B T}{Q_{t,k}} \quad (21)$$

$$\mathbf{S}_{V_r,k} = 4k_B T r_k . \quad (22)$$

The SQUID has also intrinsic noises which can be split into voltage and current noises. The determination of these noises requires the knowledge of the complete SQUID design. Therefore, we have to go beyond the description of Section 2.1.2. In particular we need the shunt resistance  $R_{sh,k}$  used to remove hysteresis, the washer inductance  $L_{SQ,k}$ , and  $M_{SQ,k}$  the mutual inductance between the SQUID input and the washer, see Figure 3.

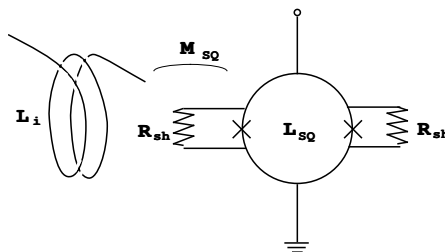


Figure 3. SQUID detail.



The SQUID voltage and current noises are, according to Clarke's model [14]

$$\mathbf{S}_{V_n,k} = 11 \frac{k_B T_{SQ,k}}{R_{sh,k}} \omega^2 M_{SQ,k}^2 \quad (23)$$

$$\mathbf{S}_{W,k} = 16 \left( \frac{L_{SQ,k}}{M_{SQ,k}} \right)^2 \frac{k_B T_{SQ,k}}{R_{sh,k}} \quad (24)$$

where  $T_{SQ,k}$  is the SQUID thermodynamic temperature.

*2.2.2. Noise matrix* The noise transducer outputs are proportional to the SQUID input current and thus given by

$$\tilde{\mathbf{I}}_i(\omega) = \mathbf{M}_i \mathbf{G}(\omega) \begin{pmatrix} \tilde{\mathbf{F}}^{\text{noise}} \\ \tilde{\mathbf{f}}^{\text{noise}} \\ \tilde{\mathbf{V}}_r \\ \tilde{\mathbf{V}}_n \end{pmatrix}(\omega) + \tilde{\mathbf{I}}_W(\omega) \equiv \mathbf{G}_I(\omega) \tilde{\mathbf{F}}(\omega) + \tilde{\mathbf{I}}_W(\omega) \quad (25)$$

where  $\tilde{\mathbf{I}}_W(\omega)$  is the SQUID noise current and  $\mathbf{M}_i$  is a  $N \times (3N + J)$  matrix given by

$$\mathbf{M}_i = \begin{pmatrix} 0_{N,J} & 0_{N,N} & 0_{N,N} & \mathbb{I}_N \end{pmatrix} \quad (26)$$

used in order to conserve only the SQUID input current and we have defined  $\mathbf{G}_I(\omega) \equiv \mathbf{M}_i \mathbf{G}(\omega)$  to simplify the notation.

Knowing the current we can compute the noises matrix  $\mathbf{S}$ , which is given by

$$\mathbf{S} = \mathbf{I}_i(\omega) \mathbf{I}_i^\dagger(\omega) = \mathbf{G}_I \tilde{\mathbf{F}} \tilde{\mathbf{F}}^\dagger \mathbf{G}_I^\dagger + \mathbf{G}_I \tilde{\mathbf{F}} \tilde{\mathbf{I}}_W^\dagger + \tilde{\mathbf{I}}_W \tilde{\mathbf{F}}^\dagger \mathbf{G}_I^\dagger + \tilde{\mathbf{I}}_W \tilde{\mathbf{I}}_W^\dagger \quad (27)$$

The matrix  $\tilde{\mathbf{F}} \tilde{\mathbf{F}}^\dagger$  is the correlation matrix of the different forces and voltages (Note that not all entries have the same units). Assuming that the different forces and voltage are only due to noises and are not-correlated this reduce to a diagonal matrix containing only autocorrelation

$$\mathbf{F} \mathbf{F}^\dagger = \text{Diag}(\mathbf{S}_F, \mathbf{S}_f, \mathbf{S}_{V_r}, \mathbf{S}_{V_n}) \quad (28)$$

The same argument leads to the cancellation of the  $\tilde{\mathbf{F}} \tilde{\mathbf{I}}_W^\dagger$  and  $\tilde{\mathbf{I}}_W \tilde{\mathbf{F}}^\dagger$  terms into (27) and to set

$$\tilde{\mathbf{I}}_W \tilde{\mathbf{I}}_W^\dagger = \text{Diag}(\mathbf{S}_W) \quad (29)$$

Therefore under the assumption that the different noises are not correlated the noise matrix (27) reduces to

$$\mathbf{S}^{\text{noise}} = \mathbf{G}_I \text{Diag}(\mathbf{S}_F, \mathbf{S}_f, \mathbf{S}_{V_r}, \mathbf{S}_{V_n}) \mathbf{G}_I^\dagger + \text{Diag}(\mathbf{S}_W) \quad (30)$$

### 2.3. Effect of a GW

The presence of a GW will manifest itself as a force acting on the sphere modes. We skip the computation (see [6]) and just note that in Fourier space the force acting on the  $j$ -th mode is

$$\tilde{F}_j^{\text{GW}} = -\frac{1}{2} \omega^2 m_s \chi_j R_s \tilde{h}_j \quad (31)$$

where  $\chi_j R_s$ , the effective length of the mode, depends only on the multiplet ( $n$ ) to which the mode belongs, and  $\tilde{h}_j$  is the projection of the (spatial part of the) GW tensor <sup>+</sup> on the  $j$ -th mode. Choosing the decomposition of the tensor on real matrix [15] we specify the form of  $\tilde{\mathbf{h}}$  for the quadrupolar modes ( $\ell = 2$ ) by\*.

$$\tilde{\mathbf{h}} = \mathbf{T}_V \begin{pmatrix} \tilde{h}_+ \\ \tilde{h}_\times \end{pmatrix} \equiv \begin{pmatrix} \frac{\sqrt{3}}{2} \sin^2 \theta & 0 \\ -\frac{1}{2} \sin 2\theta \sin \phi & \sin \theta \cos \phi \\ \frac{1}{2} \sin 2\theta \cos \phi & \sin \theta \sin \phi \\ \frac{1}{2} (1 - \cos^2 \theta) \cos 2\phi & \cos \theta \sin 2\phi \\ -\frac{1}{2} (1 - \cos^2 \theta) \sin 2\phi & \cos \theta \cos 2\phi \end{pmatrix} \begin{pmatrix} \cos 2\psi & \sin 2\psi \\ -\sin 2\psi & \cos 2\psi \end{pmatrix} \begin{pmatrix} \tilde{h}_+ \\ \tilde{h}_\times \end{pmatrix} \quad (32)$$

where  $(\theta, \phi)$  gives the arrival direction.  $\tilde{h}_+$  and  $\tilde{h}_\times$  describe the two polarization of the GW in the source frame. The actual polarization in the detector depend on the position of the source  $(\theta, \phi)$  and on the orientation of the source which is rotated by an angle  $\psi$  along the line of the sight with respect to the detector frame. We call  $\psi$  the polarization angle since for a source at a given location a change in  $\psi$  act only on the polarization.

The presence of a GW in a noise-free detector leads to an output signal given by the vector of SQUID input current

$$\mathbf{I}_{\text{sig}}(\omega) = \mathbf{G}_I(\omega) \begin{pmatrix} \tilde{\mathbf{F}}^{\text{GW}}(\omega) \\ \mathbf{0} \\ \mathbf{0} \\ \mathbf{0} \end{pmatrix} = \hat{\mathbf{G}}_I(\omega) \tilde{\mathbf{F}}^{\text{GW}}(\omega) = -\frac{1}{2} \omega^2 m_s R_s \chi \hat{\mathbf{G}}_I(\omega) \mathbf{T}_V \begin{pmatrix} \tilde{h}_+ \\ \tilde{h}_\times \end{pmatrix} \quad (33)$$

where we have assumed that all  $\chi_j$  have the same value  $\chi$  and we have defined  $\hat{\mathbf{G}}_I$ , the sub-matrix

$$\hat{\mathbf{G}}_I = \mathbf{G}_I \begin{pmatrix} \mathbb{1}_J \\ 0_{N,J} \\ 0_{N,J} \\ 0_{N,J} \end{pmatrix} = \underbrace{\begin{pmatrix} 0_{N,J} & 0_{N,N} & 0_{N,N} & \mathbb{1}_N \end{pmatrix}}_{N \times (3N+J)} \mathbf{G} \underbrace{\begin{pmatrix} \mathbb{1}_J \\ 0_{N,J} \\ 0_{N,J} \\ 0_{N,J} \end{pmatrix}}_{(3N+J) \times J} \quad (34)$$

#### 2.4. Detector sensitivity

The detector sensitivity is given by the comparison between the output due to the noise and the one due to a GW. The output of the detector is given by  $N$  output currents (one by transducer). One can combine theses outputs in different way. The ability of extracting the GW signal depends on the way the outputs are combined and so do the sensitivity.

*2.4.1. Single transducer analysis* In this first data analysis schema, we considered a rather naive way of using the different transducers: each one is taken as an independent experiment. This has the advantage of simplifying drastically the data analysis (which

<sup>+</sup> By a GW tensor we mean the perturbation of the background metric in the TT gauge

\* Note that if we describe gravitation by general relativity, only spheroidal quadrupolar modes ( $l = 2$ ) have non zero  $\tilde{h}_j$

can be based on the one of the resonant bar without further modifications). However it is clear that in this way we are losing most of the advantages of the spherical geometry. Nevertheless it is instructing to perform this analysis having in mind that it will probably be useful in the first phase of any sphere experiment.

If we are looking only at the  $k$ -th transducer, its noise spectral density is given by the diagonal components of (30)

$$S_{I_i^k} = \mathbf{S}^{kk} = \sum_{\ell=1}^j |\mathbf{G}_{J+2N+k,\ell}|^2 \mathbf{S}_{F,\ell} + \sum_{\ell=1}^N |\mathbf{G}_{J+2N+k,J+\ell}|^2 \mathbf{S}_{f,\ell} + \sum_{\ell=1}^N |\mathbf{G}_{J+2N+k,J+N+\ell}|^2 \mathbf{S}_{V_n,\ell} + \sum_{\ell=1}^N |\mathbf{G}_{J+2N+k,J+2N+\ell}|^2 \mathbf{S}_{V_r,\ell} + \mathbf{S}_W^k \quad (35)$$

and this has to be compared with the spectral density of the  $k$ -th SQUID input current due to the GW. The latter is obtained as the square of the equ. (33)

$$S_k^{GW} = \frac{1}{4} \omega^4 m_s^2 R_s^2 \chi^2 \left| \sum_{\ell m} \mathbf{G}_I^{k\ell r} \mathbf{T}_V^{\ell m} \begin{pmatrix} \tilde{h}_+ \\ \tilde{h}_\times \end{pmatrix} \right|^2 \quad (36)$$

If we know the GW arrival direction, we can compute each  $\mathbf{T}_V$  and simulate the detector response. The inverse problem, computing the GW propagation direction, needs high signal to noise ratio (SNR) [17]. If we are interested in the detector sensitivity we are working at SNR=1, and therefore we have no information on the arrival direction. Furthermore, if we choose an arbitrary direction we can be in a case where some of the modes are poorly or not at all coupled to this peculiar GW. Consequently we can underestimate the sensitivity ‡. As the spectral density is a statistical feature of the signal, it is then natural to perform an average on the possible arrival directions and over the source orientation (polarization angle).

Averaging  $S_k^{GW}$  over the arrival direction  $(\theta, \phi)$  and the source orientation (polarization angle  $\psi$ ) and assuming an intrinsic polarization  $\tilde{h}_+ \equiv \tilde{h}$ ,  $\tilde{h}_\times \equiv 0$ , we find [19]

$$S_k^{GW} = \frac{1}{10} \omega^4 m_s^2 R_s^2 \chi^2 \tilde{h}^2 \sum_{\ell=1}^5 \mathbf{G}_{J+2N+k,\ell}^2 \quad (37)$$

The strain sensitivity is given by the comparison  $S_{I_i^k} = S_k^{GW}$  and is

$$\tilde{h}_c(\omega) = \left( \frac{S_{I_i^k}}{\frac{1}{20} \omega^4 m_s^2 R_s^2 \chi^2 \sum_{\ell=1}^5 \mathbf{G}_{J+2N+k,\ell}^2} \right)^{1/2} \equiv \left( \frac{S_{I_i^k}(\omega)}{T_F(\omega)} \right)^{1/2}, \quad (38)$$

where we have defined the transfer function  $T_F$ .

‡ As an illustration: the case of a cylindrical detector. If we choose the GW arrival direction parallel to the detector axis, the GW is not seen and no information is given about the detector sensitivity.

2.4.2. *Coherent analysis* Rather than looking at each transducer separately we can perform a coherent analysis taking into account all the  $N$  signals. In this case we have to perform multidimensional matched filtering [17]. In the special case of TIGA configuration, one can use the mode channels in order to obtain directly the motion of the quadrupolar modes of the sphere [6]. However, on one hand, this property was proved for the sphere with mechanical resonators and may be affected by the tuned electric oscillators and/or by the perturbations induced by the suspension of the sphere in the Earth gravity. On the other hand, having the motion of the sphere modes is not enough: one has to make the deconvolution between the excitations and the damped motion of the modes.

If, for a given transducer number and configuration, we know the detector response to an excitation, one can directly build a multidimensional matched filter [18]. One can therefore achieve optimal filtering (once the waveform of the GW is known or assumed to be known). Note that the construction of the filter can be performed using our numerical model, see [18] for details.

The multidimensional matched filtering can be defined and used for *any* configuration but in general it has to be computed numerically. However the TIGA configuration offers the great advantage of accepting analytic solutions to the deconvolution problem. In the following, thanks to a result of Stevenson [17], we do not need to know how the matched filtering will be performed and whether the filter is obtained in a numerical or analytical way. We only need to know that an optimal filter is applied to the data. In this case the SNR is given by [17]

$$SNR = \int_{-\infty}^{\infty} \sigma(\omega) d\omega / 2\pi \quad (39)$$

$$\sigma(\omega) = \mathbf{I}_{\text{sig}}^\dagger(\omega) \mathbf{S}^{-1}(\omega) \mathbf{I}_{\text{sig}}(\omega) \quad (40)$$

where  $\mathbf{S}$  is the noise matrix defined by equation (27).

Using the expressions (33), we get

$$\sigma(\omega) = \frac{1}{4} \omega^4 m_s^2 R_s^2 \chi^2 \begin{pmatrix} \tilde{h}_+^* & \tilde{h}_\times^* \end{pmatrix} \mathbf{T}_V^\dagger \underbrace{\hat{\mathbf{G}}_I^\dagger \mathbf{S}^{-1} \hat{\mathbf{G}}_I}_{\mathbf{H}} \mathbf{T}_V \begin{pmatrix} \tilde{h}_+ \\ \tilde{h}_\times \end{pmatrix} \quad (41)$$

In order to evaluate this expression we face again the problem that  $\mathbf{T}_V$  is a function of the arrival direction and of the source orientation. As in the single transducer analysis it is convenient to average the expression over the direction and the polarization. This gives

$$\begin{aligned} \left\langle \begin{pmatrix} \tilde{h}_+ \\ \tilde{h}_\times \end{pmatrix}^\dagger \mathbf{T}_V^\dagger \mathbf{H} \mathbf{T}_V \begin{pmatrix} \tilde{h}_+ \\ \tilde{h}_\times \end{pmatrix} \right\rangle &= \int_0^\pi \int_0^{2\pi} \frac{\sin(\theta) d\theta d\phi}{4\pi} \int_0^\pi \frac{d\psi}{\pi} \begin{pmatrix} \tilde{h}_+ \\ \tilde{h}_\times \end{pmatrix}^\dagger \mathbf{T}_V^\dagger \mathbf{H} \mathbf{T}_V \begin{pmatrix} \tilde{h}_+ \\ \tilde{h}_\times \end{pmatrix} \\ &= \frac{1}{5} \text{Tr}(\mathbf{H}) (\tilde{h}_+^2 + \tilde{h}_\times^2) \end{aligned} \quad (42)$$

assuming again a polarized GW  $\tilde{h}_+ \equiv \tilde{h}$ ,  $\tilde{h}_\times \equiv 0$  we get for  $\langle \sigma \rangle$

$$\langle \sigma \rangle = \frac{1}{20} \omega^4 m_s^2 R_s^2 \chi^2 \tilde{h}^2 \text{Tr}(\mathbf{H}) \quad (43)$$

The strain sensitivity (averaged on the sky and the source orientation) is then given by solving the equation  $\langle \sigma \rangle \equiv 1$  for  $\tilde{h}(\omega)$ . We eventually obtain

$$\tilde{h}_c(\omega) = \frac{2\sqrt{5}}{\omega^2 m_S R_S \chi \sqrt{\text{Tr}(\mathbf{H})}} \quad (44)$$

### 3. Second part: application and simulations

#### 3.1. The filled sphere

We start with the case of a filled sphere, this case is easier to compare with existing computations [8] and can be used as a benchmark for the hollow sphere simulations. We also use this simple case in order to highlight the how the single transducer sensitivity is modified by the presence of other transducers. With a numerical code, implementing (12),(15-24),(35), (38), and (44), we can compute the strain sensitivity for a spherical resonant mass with capacitive transducers coupled to a dc-SQUID with input transformer and resonances frequency of the transducer tuned in order to monitor the five quadrupolar modes. The parameters used in our simulation can be found in the Table 1.

*3.1.1. Single transducer results* In the case of a single transducer analysis, we obtain  $N$  sensitivity curves – one for each transducer. As an example we considerate a 1[m] radius bulk CuAl sphere with 6 transducers in TIGA configuration. At the quantum limit, the typical strain sensitivity of one of the transducers is plotted in Figure 4. Note the presence of horns on the both side of the resonance. We can understand them as the contribution from the noises of the 5 others transducers. This explanation is confirmed by the sensitivity curves obtained for the same sphere but with a different number of transducers, see Figure 5. As we increase the number of transducers we also increase the number of noise sources, and the sensitivity of a single transducer is worse than if the sphere was equipped with a single transducer. Although this finding is not surprising and can be related to existing literature [23, 24], the details of this feature are important in order to calibrate the transducers.

*3.1.2. Coherent analysis results* We now work out the coherent strain sensitivity for the same sphere as in the previous case. For 6 transducers placed into a TIGA configuration the sensitivity does not present horns as show in Figure 6. We also plot the sensibility corresponding to the best present transducer ( $N_{phonon} = 50$ ).

One can address the question of understanding how the sensitivity is modified if we change the number of transducers. As the sphere with a single transducer has the same pattern function as a bar, we can expect that each new transducer partially complete the coverage of the polarization and arrival directions until for  $N = 5$  we have a omnidirectional and omni-polarization detector. The sensitivity will then be improved by the addition of each transducer. Furthermore we will add the transducers in order

Sphere	Radius Mass Quality factor Number of modes Modes frequencies Radial eigen-function Ratio effective/real radius	$R_s = 1[m]$ $m_s = 33091[kg]$ $Q_s = 5 \cdot 10^7$ $J = 5$ $\frac{\omega_{s,j}}{2\pi} = 1049, 1053, 1057, 1061, 1065 [Hz]$ $\alpha = -2.89$ $\chi = 0.328$
Transducer	Mass Quality factor Resonator frequencies Field in the capacity Capacities Transformer primary inductance Transformer secondary inductance Transformer mutual inductance Transformer resistance	$m_t = 165[kg]$ $Q_t = 5 \cdot 10^7$ $\frac{\omega_{t,k}}{2\pi} = 1046, 1051, 1055, 1059, 1063, 1068 [Hz]$ $E = 4.5 \cdot 10^7[V/m]$ $C_{t,k} = 36.9, 36.7, 36.4, 36.1, 35.8, 35.5 [nF]$ $L_p = 1.3[H]$ $L_s = 8 \cdot 10^{-6}[H]$ $M = 2.6 \cdot 10^{-3}[H]$ $r_k \sim 2.9 \cdot 10^{-4}[\Omega]$
SQUID	Input inductance Washer inductance Shunt resistance Mutual inductance	$L_i = 1.7 \cdot 10^{-6}[H]$ $L_{SQ} = 80 \cdot 10^{-12}[H]$ $R_{sh} = 4[\Omega]$ $M_{SQ} = 10[nH]$

**Table 1.** Parameter values for the filled sphere at the quantum limit. If the mode ( $j$ ) or transducer ( $k$ ) indices is absent, it means that the same value is used for all the indices range. The frequency splitting in  $\omega_{s,j}$  is extrapolated from the miniGRAIL one. The capacities  $C_{t,k}$  are chosen in order to tune the electric frequencies on the resonator ones. The transformer resistance is computed in order to get a electrical quality factor  $Q_e = 5 \cdot 10^7$ . The temperature and the SQUID effective temperature are fixed to  $20[mK]$ .

to complete a TIGA configuration and therefore, due to the particular symmetry of this configuration, we expect the complete TIGA configuration to be even more sensitive than the incomplete 5-transducers one. The simulations confirm this analysis as shown in Figure 7.

### 3.2. The hollow sphere

All the above treatment has a nice, simple generalization to the case of a hollow sphere [20]. While preserving all the feature of a bulk sphere such as omnidirectionality, and the capability to determine the source direction and wave polarization, an hollow sphere has several interesting peculiar properties. Its quadrupole frequencies are lower than those of an equally massive solid sphere, thus making the low-frequency range accessible to this antenna with good sensitivity. Further, as shown in [20], for an appropriate ratio between the inner and outer diameter, the cross section for the second quadrupole mode

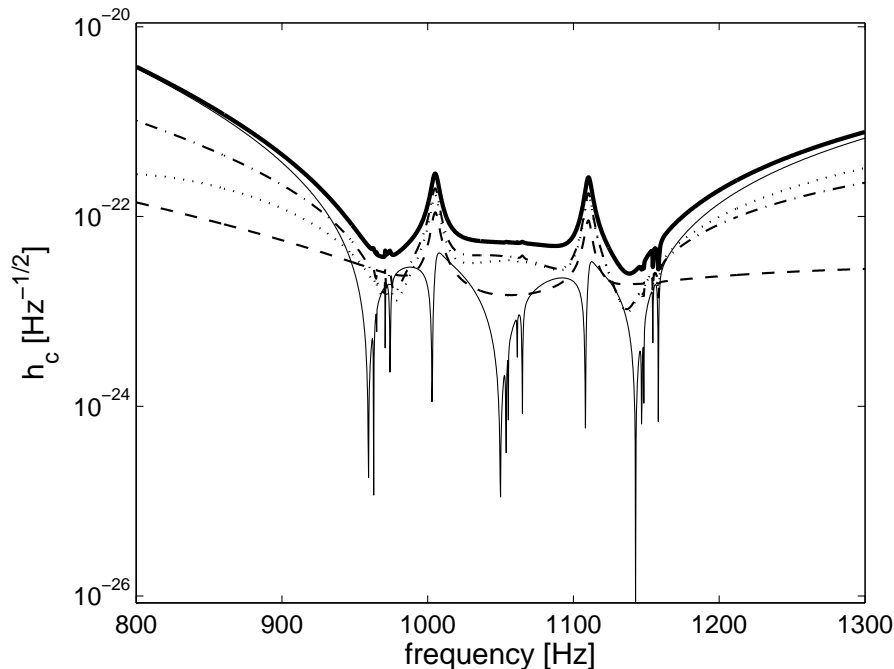


**Figure 4.** Strain sensitivity at the quantum limit for one of the 6 transducers placed into a TIGA configuration on a 1[m] radius bulk CuAl sphere. The curves are the relative contributions of the different noises: the thick line is the total sensitivity, the dashed curve is the mechanical thermal noise contribution (20,21), the dashed-dotted line is the thermal electric noise contribution (22), the dotted line the back-action contribution (23) and the continuous curve the white noise (24).

equals that of the first, and one has the possibility of working with a detector with the same (high) sensitivity at two frequencies. The main differences with the bulk sphere are the numerical values of the radial functions  $\alpha_j$ , that we first met in equation (9), and the one of the coupling to GW, namely  $\chi$  (see equation (31)). We have also to recompute the eigen-frequencies (this can be done using the formulas from ref. [20]). We have applied our model to a 1[m] external radius and  $a = 0.4[m]$  internal radius hollow sphere, with 6 transducers in the TIGA configuration coupled to the first quadrupolar modes. The results of our computation are displayed in the Table 2. The corresponding coherent strain sensitivity at the quantum limit is show In Figure 8. Note that the frequency window is shifted by about 200[Hz] with respect to the filled sphere and that the sensitivity loss is only by about a factor 1.5.

*3.2.1. Effect of the thickness of the hollow sphere* We address now the question of the influence of the thickness of the sphere on its sensitivity. For a fixed external radius a thinner sphere is less massive, and therefore less sensitive. There is also a shift in the resonances to lower frequencies when the sphere is thinner, see Figure 9.

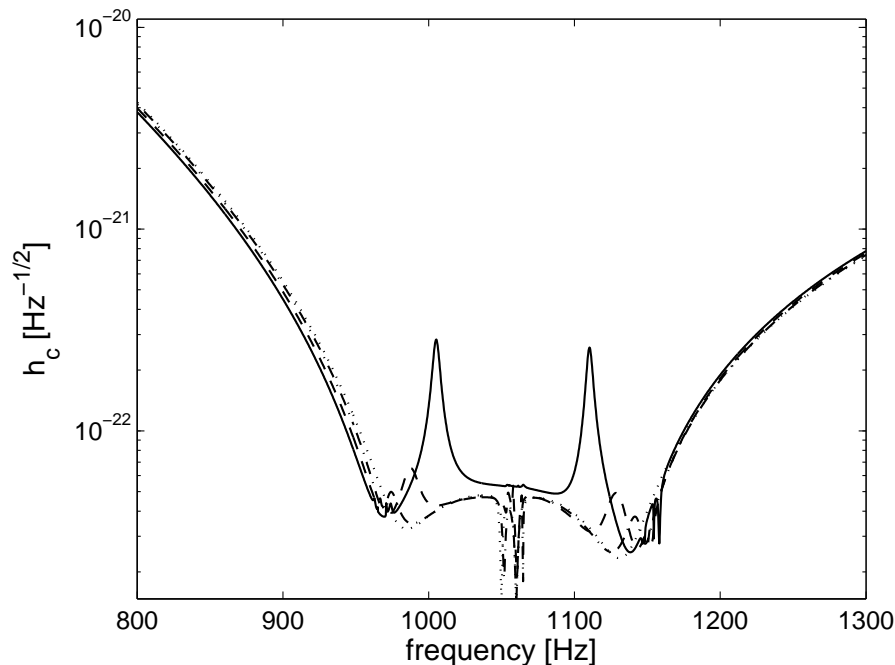


**Figure 5.** Strain sensitivity for the single transducer analysis. The purpose of this figure is to show the effect of the noise due to the presence of other transducers. The dotted curve is the sensitivity for a single transducer on a 1[m] radius bulk CuAl sphere. Then, always performing the analysis of the output of one transducer we add others transducers acting as noises sources: the dashed-dotted curves stand for a sphere with 2 transducers on the 2 first TIGA locations, the dashed curves for a set of 4 transducers on the 4 first TIGA locations, and the continuous curve is the sensitivity for a transducer out of a 6 transducer TIGA configuration. Note how the presences of further noises sources (= the other transducers) deteriorate the sensitivity by adding horns.

*3.2.2. Enlarging the bandwidth by monitoring the second quadrupolar multiplet* We now compare different designs of multi-modal resonant detectors based on a hollow sphere. We will always work on the base of our 0.4/1[m] hollow sphere described above and we compare different transducers designs.

Having a description of the hollow sphere with 6 transducers monitoring the first quadrupolar multiplet we can now simulate a multi-modal detector. As discussed in Section 2.1.4, we have to take into account the presence of other sphere modes. In Table 3, we list the properties of the modes we include in the simulation of our multi-modal models. Each modes multiplet  $(n, \ell)$  contain  $2\ell + 1$  modes and therefore we take into account a total of  $J = 30$  spheroidal modes in our simulations. Only 10 of them are coupled to GW.

For a hollow sphere, we have the choice of placing the transducers on the outer or on the inner surface (this choice may be limited by the experimental difficulty of placing transducers inside the sphere). Looking only at the quadrupolar modes, and because



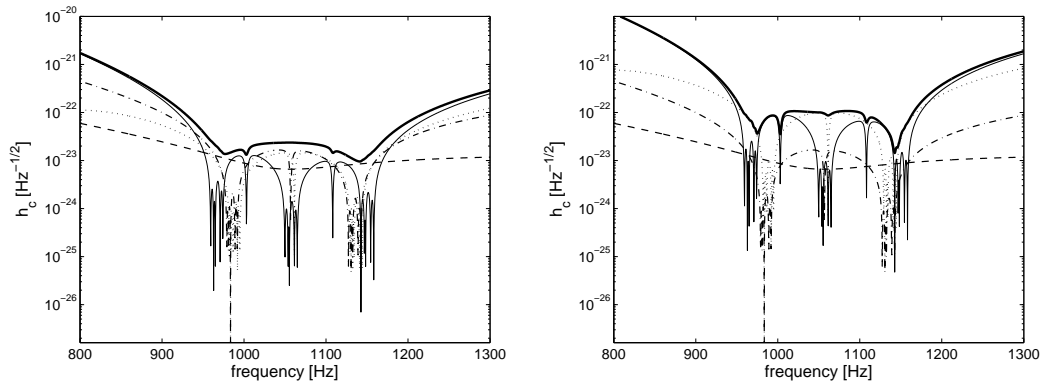


**Figure 6.** Strain sensitivity at the quantum limit (left) and for  $N_{phonon} = 50$  (right) for a coherent analysis of the outputs of 6 transducers placed into a TIGA configuration on a 1[m] radius bulk CuAl sphere. The curves are the relative contributions of the different noises: the thick line is the total sensitivity, the dashed curve is the mechanical thermal noise contribution (20,21), the dashed-dotted line is the thermal electric noise contribution (22), the dotted line the back-action contribution (23) and the continuous curve the white noise (24).

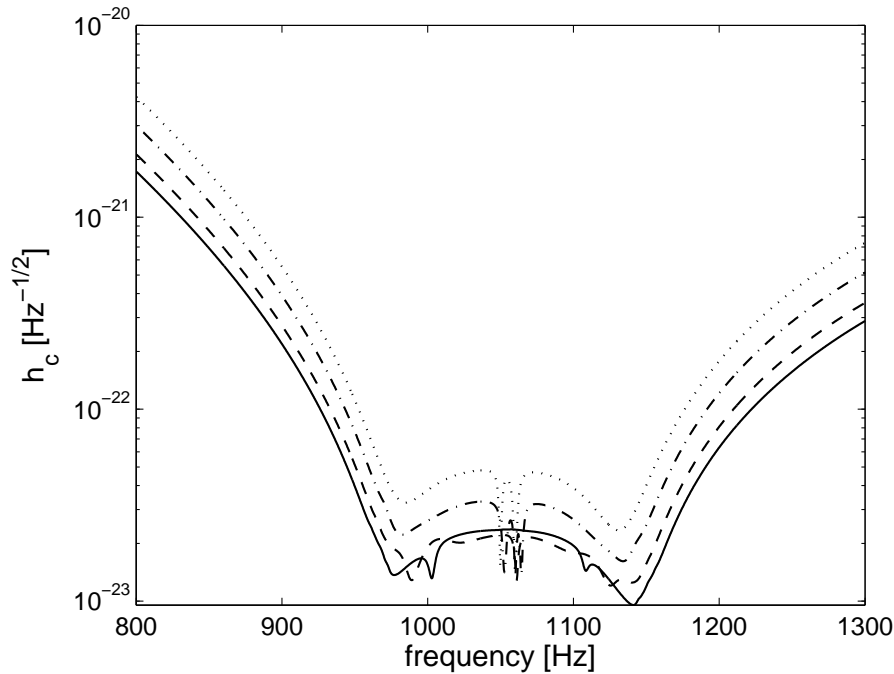


**Figure 7.** Coherent strain sensitivity at the quantum limit of a transducer set placed on a 1[m] radius bulk CuAl sphere. The continuous curve is the sensitivity for a 6 transducers TIGA configuration, the dashed curves the one for a set of 4 transducers on the 4 first TIGA location the dashed-dotted curves the one for a set of 2 transducers on the 2 first TIGA location and the dotted curve is the sensitivity for a single transducer. (Note that the dotted curve is the same as in Figure 5)

Sphere	Radius	$R_s = 1[m]$
	Internal radius	$a = 0.4[m]$
	Mass	$m_s = 30974[kg]$
	Modes frequencies	$\frac{\omega_{s,j}}{2\pi} = 861, 865, 869, 873, 877 [Hz]$
	Radial eigen-function	$\alpha = -2.73$
	Ratio effective/real radius	$\chi = 0.322$
Transducer	Mass	$m_t = 155[kg]$
	Resonator frequencies	$\frac{\omega_{t,k}}{2\pi} = 859, 863, 867, 871, 875, 879 [Hz]$
	Field in the capacity	$E = 4.5 \cdot 10^7[V/m]$
	Capacities	$C_{t,k} = 55, 54, 54, 53, 53, 52 [nF]$
	Transformer resistance	$r_k \sim 2.4 \cdot 10^{-4}[\Omega]$

**Table 2.** Parameters value for the hollow sphere with  $a = 0.4[m]$  internal radius at the quantum limit. The transducer being build on the same model as for the filled sphere we put in this table only the quantities which differ from the filled case. The temperature and the SQUID effective temperature are fixed to  $20[mK]$ . The other values can be found into the Table 1.

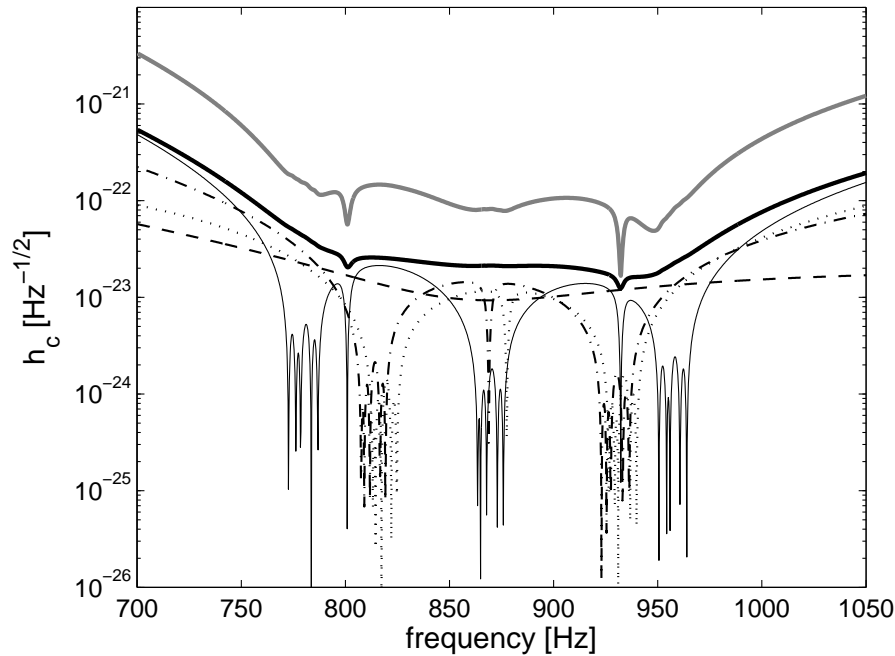


**Figure 8.** Coherent strain sensitivity at the quantum limit for a set of 6 transducers placed in a TIGA configuration on a  $0.4[m]/1[m]$  internal/external radius CuAl sphere. The curves are the relative contributions of the different noises (see Figure 4). The gray curve is the sensibility corresponding to the best present transducer ( $N_{phonon} = 50$ ).

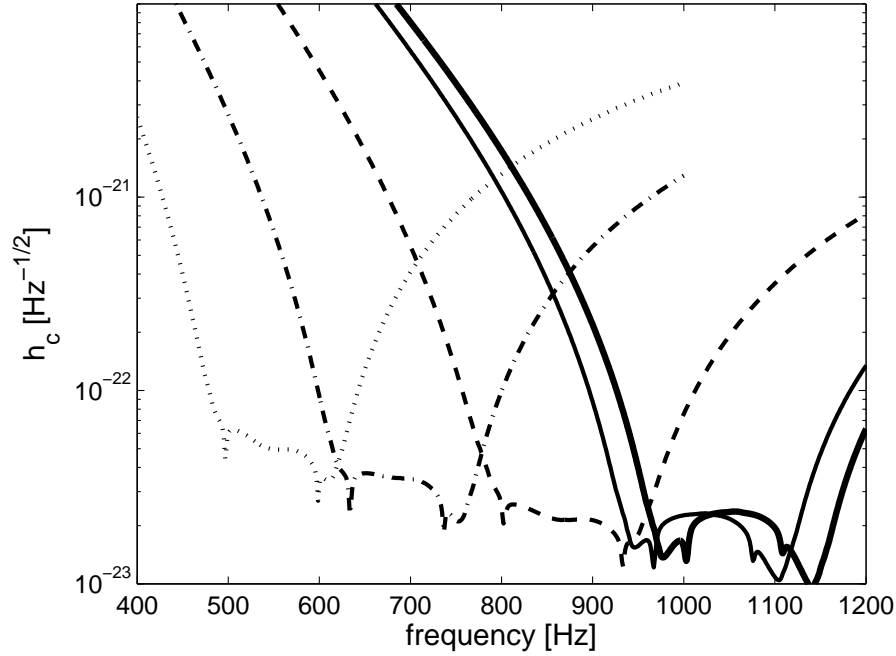


**Figure 9.** Coherent strain sensitivities at the quantum limit for a TIGA configuration on a 1[m] external radius hollow CuAl sphere for different values of the internal radius  $a$ . The dotted curve is for  $a = 0.8[m]$  (ie. a shell of thickness 0.2[m]) the successive curves are for  $a$  decreasing by step of 0.2[m] until the black thick line which stand for the filled sphere.

$n, \ell$	$f_{n,\ell}$	$\alpha_{n,\ell}(R_S)$	$\alpha_{n,\ell}(a)$	$\chi_{n,\ell}$
(1,2)	869[Hz]	-2.73	-2.85	0.319
(1,3)	1421[Hz]	-0.488	17.1	0
(1,1)	1558[Hz]	-1.41	-4.02	0
(1,0)	1758[Hz]	-1.29	-1.06	0
(1,4)	1937[Hz]	1.51	21.1	0
(2,2)	1970[Hz]	0.276	-3.27	-0.148
other	>2.4[kHz]			

**Table 3.** Frequency, radial eigen-function (at the outer and inner surface) and coupling to GW for the first modes of a hollow sphere with external radius  $R_S = 1[m]$  and internal radius  $a = 0.4[m]$ . All these quantities are computed from formulas found in [20].

the radial displacement of the second mode is maximum at the inner side of the sphere [20], one could think of improving the sensitivity by mounting the classical capacitive transducers considered here inside the sphere. However, as show in Table 3, the higher multipolar modes have very large  $\alpha$ 's on the inner surface. These modes will couple to the transducers main resonances and their thermal noise will eventually limit the detector sensitivity. This effect is analysed in detail below.

A first approach to design a multi-modal spherical detector is to add a second set of 6 transducers in TIGA configuration coupled to the second quadrupolar multiplet. The characteristic of the second set of transducer are listed in Table 4. The parameters are optimized to get the best strain sensitivity and the largest bandwidth following the detailed analysis for a bulk sphere reported in [12, 13]. We notice that the optimal mass of the resonator coupled to the second quadrupolar modes is smaller that the first resonator. This is due to the fact that the effective mass of the higher quadrupolar modes is smaller and the higher frequencies of the modes requires a smaller transducer mass to have the same electro-mechanical coupling. In our simulation we can choose to place the transducers inside or outside the sphere. On Figure 10 we show the difference in the strain sensitivity for a hollow sphere with 12 transducers when the thermal noise contribution of all the modes between the first and second quadrupolar multiplet is included. Both the configurations with the second set of transducers placed outside and inside the sphere are considered. The thermal noise of the modes not coupled to GW reduces slightly the bandwidth in the former case, but has dramatic effect on the sensitivity in the latter case.

Mass	$m_{t,k=7..12} \sim \frac{1}{5}m_{t,k=1..6} = 31[kg]$
Resonator frequencies	$\frac{\omega_{t,k}}{2\pi} = 1947, 1956, 1965, 1974, 1983, 1992 [Hz]$
Field in the capacity	$E = 4.5 \cdot 10^7[V/m]$
Capacities	$C_{t,k} \sim 10 [nF]$
Transformer resistance	$r_k \sim 5.4 \cdot 10^{-4}[\Omega]$

**Table 4.** Parameter values for the second set of transducers. For comments, see Table 1 and for the sphere parameters see Table 2 and 3 .

From Figure 10 one can conclude that placing the transducers inside the sphere will not lead to an improvement of the sensitivity. We observe that a 12 transducers in 2 TIGA configuration on the outer surface of a 0.4/1[m] hollow sphere can lead to a sensitivity curve with 2 windows below  $3 \cdot 10^{-23}[Hz^{-1/2}]$  with bandwidth of 175 and 52[Hz].

Having in mind that the presence of 12 transducers can represent an experimental problem (even on the outer surface of the sphere), we now consider the possibility of reducing the number of transducers by using the double-mode transducer described in Section 2.1.3. We then perform simulations of a multi-modal spherical GW detector with only 6 double-mode transducers in a TIGA configuration.

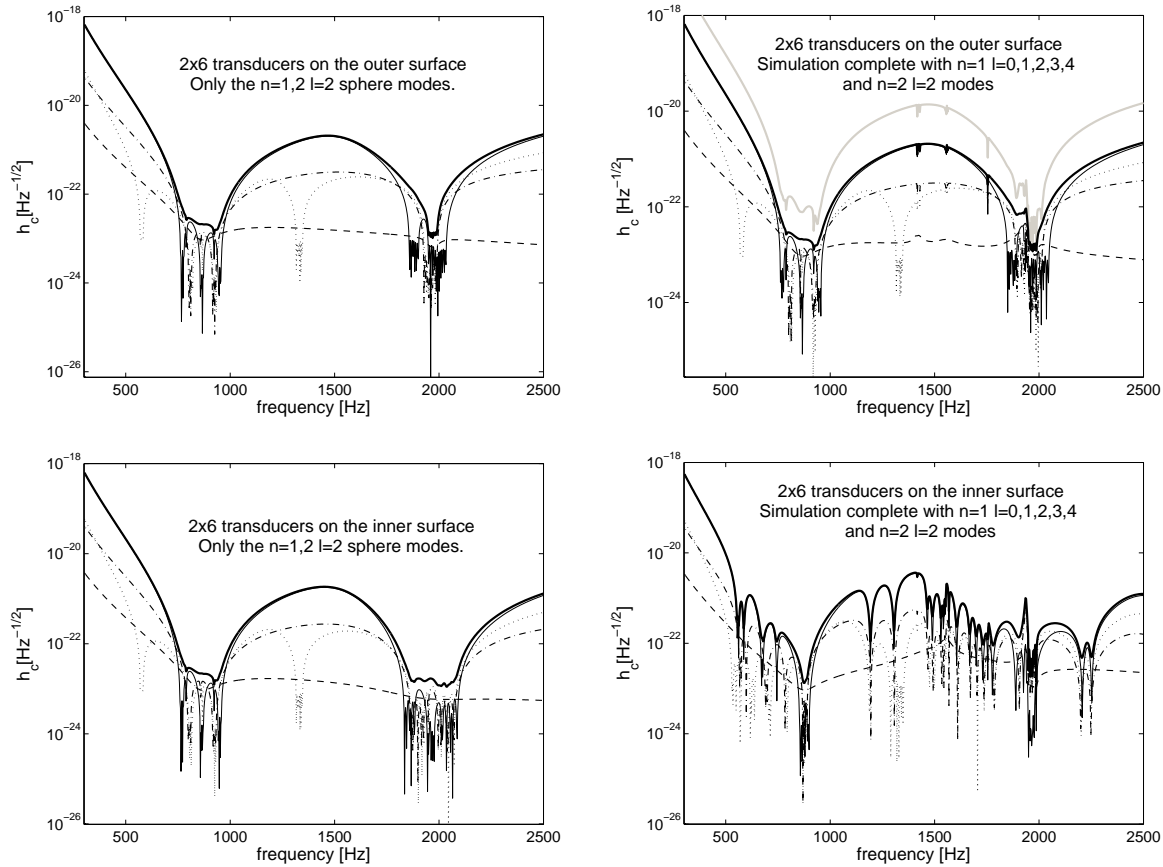


**Figure 10.** Coherent strain sensitivity at the quantum limit for two sets of 6 transducers placed in TIGA configuration on a  $0.4\text{[m]}/1\text{[m]}$  internal/external radius CuAl sphere. Each transducer set is coupled to the first and second quadrupolar modes, respectively. The curves show the relative contributions of the different noises: the black thick line is the total sensitivity, the dashed curve is the total mechanical thermal noise contribution (20,21), the dashed-dotted line is the thermal electric noise contribution (22), the dotted line the back-action contribution (23) and the continuous curve the white noise (24). The left panels are the result of the simulations with only the quadrupolar sphere modes, in the right panel we have add the other modes with frequency smaller than  $2.5\text{[kHz]}$ . The upper plots are for transducers on the outer surface and the lower ones are for transducer on the inner surface. On the upper right plot the gray curve is the sensitivity for  $N_{\text{phonon}} = 50$

In figure 11 we show the sensitivity of a hollow sphere equipped with 6 double-mode transducers. The transducers parameters, reported in Table 5, are chosen to get the best sensitivity and the largest bandwidth at the two principal quadrupolar modes multiplets around 800 and 1900 Hz. The choice of the parameters in Table 5 is the result of an iterative process based on the detailed optimization procedure described in [12, 13] for a bulk sphere. A more detailed technical analysis is necessary to fully optimized the detector described here. Such an analysis is beyond the scope of this paper.

The sensitivity around the two most sensitive spheroidal modes is comparable with

Mass	$m_{t,k=7..12} \sim \frac{1}{5}m_{t,k=1..6} = 31[kg]$
Quality factor	$Q_{t1} = Q_{t2} = 5 \cdot 10^7$
Resonator frequencies	$\frac{\omega_{t1}}{2\pi} = 859, 863, 867, 871, 875, 879 [Hz]$
Field in the capacity	$\frac{\omega_{t2}}{2\pi} = 1947, 1956, 1965, 1974, 1983, 1992 [Hz]$
Capacities	$E_1 = E_2 = 4.5 \cdot 10^7 [V/m]$
Transformer primary inductance	$C_{1,k} \sim 35 [nF]$
Transformer secondary inductance	$C_{2,k} \sim 10 [nF]$
Transformer mutual inductance	$L_{1,p} = L_{2,p} = 1.3[H]$
Transformer resistance	$L_{1,s} = L_{2,s} = 8 \cdot 10^{-6}[H]$
	$M_1 = M_2 = 2.6 \cdot 10^{-3}[H]$
	$r_{1,k} \sim 2.4 \cdot 10^{-4}[\Omega]$
	$r_{2,k} \sim 5.4 \cdot 10^{-4}[\Omega]$
Input inductance	$L_i = 1.6 \cdot 10^{-6}[H]$
Washer inductance	$L_{SQ} = 80 \cdot 10^{-12}[H]$
Shunt resistance	$R_{sh} = 4[\Omega]$
Mutual inductance	$M_{SQ} = 10[nH]$

**Table 5.** Parameters value for the set of double modes transducers. For comments see Table 1 and for the sphere parameters see Table 2 and 3.

the one obtained with a 12 single-mode transducers configuration. Thanks to the use of a single SQUID to amplify the signal from both the spheroidal modes families, the resulting back-action noise contribution of the SQUID amplifiers is reduce in the double-transducer read-out scheme. This leads to a larger bandwidth at the second spheroidal mode frequencies. Between the two modes families the sensitivity is reduced due to a low mechanical coupling between the resonators and the sphere modes, and is limited by the additive SQUID white noise. A strain sensitive level of about  $10^{-22} Hz^{-1/2}$  and a total bandwidth of about 600 Hz could be achieved in this way around 800 and 2000 Hz. At the sensitivity of the currently best performing resonant bar antenna [4], a multimodal hollow spherical detector could reach a bandwidth of about 1kHz.

### 3.3. Concluding remarks

We developed a mathematical framework, which can describe the indirect coupling of the transducers through the modes of the sphere. We have shown how to build models giving the strain sensitivity of a GW spherical detector and presented different configurations of a multi-mode spherical resonant detector. The effect of the thermal noise from higher frequency modes of the sphere, not coupled to GW, are also included in the model. We fully analyzed the strain sensitivity of an hollow CuAl sphere of 0.4[m]/1[m] internal/external radius. Such an antenna, equipped with 12 ‘standard’ transducers or 6 double-mode transducers, when optimally tuned, may display a sensitivity curve, at the quantum limit, below  $3 \cdot 10^{-23} [Hz^{-1/2}]$  with a total bandwidth up to 600 Hz around

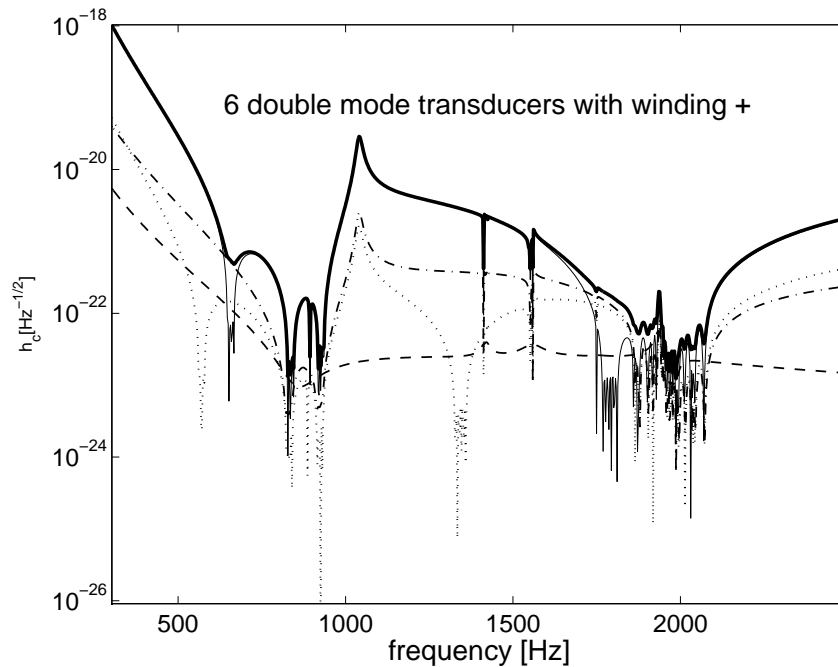


**Figure 11.** Coherent strain sensitivity at the quantum limit for a set of 6 double-mode transducers placed in TIGA configuration on a 0.4[m]/1[m] internal/external radius CuAl sphere. The curves show the relative contributions of the different noises: the black thick line is the total sensitivity, the dashed curve is the total mechanical thermal noise contribution (20,21), the dashed-dotted line is the thermal electric noise contribution (22), the dotted line the back-action contribution (23) and the continuous curve the white noise (24). All the spheroidal modes with frequency smaller than 2.5[kHz] are included in the simulation.

the first two quadrupolar multiplets at about 800 and 2000 Hz. At the sensitivity of the currently best performing resonant bar antenna [4], a multimodal hollow spherical detector could reach a bandwidth of about 1kHz. Such a detector could have peak sensitivity comparable with the first generation of interferometers, but would be also able to determine the GW arrival direction. With an appropriate resizing of the sphere, the second quadrupolar modes can be shifted to the frequency region where existing small spherical detectors are sensitive. This would open the possibility of coincidence search between several spherical detectors and the DUAL detector [21], building in this way the base for a powerful omnidirectional gravitational wave observatory.

## Acknowledgements

We wish to acknowledge M. Maggiore, S. Foffa, M.A. Gasparini, C. Caprini, A. Malaspina and L. Bonaccini for many useful discussions.

The work of J.E. is partially supported by the Swiss National Funds. The work of F.D. is supported by the Swiss National Funds and by the National Science Foundation under

Grant No. PHY99-07949. The work of L.G. was partially supported by the Integrated Large Infrastructures for Astroparticle Science (ILIAS) of the Sixth Framework Program of the European Community when the author was employed at Leiden University.

- [1] ALLEGRO - [gravity.phys.lsu.edu](http://gravity.phys.lsu.edu) , AURIGA - [www.auriga.inl.infn.it](http://www.auriga.inl.infn.it) ,  
MARIO SCHENBERG - [www.das.inpe.br/~graviton/English](http://www.das.inpe.br/~graviton/English) ,  
MiniGRAIL - [www.minigrail.nl](http://www.minigrail.nl) , ROG - [www.lnf.infn.it/esperimenti/rog/index.html](http://www.lnf.infn.it/esperimenti/rog/index.html) ,  
GEO - [www.geo600.uni-hannover.de](http://www.geo600.uni-hannover.de) , LIGO - [www.ligo.caltech.edu](http://www.ligo.caltech.edu) ,  
LISA - [lisa.jpl.nasa.gov](http://lisa.jpl.nasa.gov) , TAMA - [tamago.mtk.nao.ac.jp](http://tamago.mtk.nao.ac.jp) ,  
VIRGO - [www.virgo.infn.it](http://www.virgo.infn.it)
- [2] IGEC - <http://igec.inl.infn.it> , LIGO-TAMA - ArXiv:gr-qc/0512078
- [3] See for example: B. Abbott et al. (LSC), Phys. Rev. D **72**, 042002 (2005).
- [4] L. Baggio et al, Phys. Rev. Lett. **94** (2005) 241101.
- [5] E. Coccia and V. Fafone, Phys. Lett. A **213**, 16 (1996).
- [6] S.M. Merkowitz and W.W. Johnson, Phys. Rev. D **51**, 2546 (1995)  
S.M. Merkowitz and W.W. Johnson, Phys. Rev. D **56**, 7513 (1997)
- [7] J. A. Lobo and A. Montero, Class. Quant. Grav. **19** (2002) 6405
- [8] C. Frajuca et all, Class.Quant.Grav.21 (2004) S1107-S1111.
- [9] A. de Waard et al, Class.Quant.Grav.22, S215 - S219 (2005).
- [10] P.F. Michelson and C.Y. Zhou, Phys. Rev. D **51**, 2517 (1994)
- [11] J. A. Lobo, Phys. Rev. D **52** (1995) 591. see also ArXiv:gr-qc/0006055 for an updated version.
- [12] L. Gottardi, Transducers and low noise two-stage SQUID amplifiers for the spherical gravitational wave antenna MiniGRAIL, PhD thesis, Lion, Universiteit Leiden, Nederland (2004)
- [13] L. Gottardi, Phys. Rev. D **75** (2007) 022002. - See also ArXiv:gr-qc/0608097
- [14] Tesche, CD and Clarke, J., J. Low Temp. Phys. **29**, 301 (1977).  
Tesche, CD and Clarke, J., J. Low Temp. Phys. **37**, 397 (1979)
- [15] M. A. Gasparini, Phys. Rev. D **72**, 104012 (2005).
- [16] M. Maggiore, "Gravitational Waves, Vol I, Theory and Experiments", Oxford University Press, to appear.
- [17] T.R. Stevenson, Phys. Rev. D **56**, 7513 (1997)
- [18] M. A. Gasparini, F. Dubath, Phys. Rev. D **74**, 122003 (2006).
- [19] J. Extermann, Sur la sensibilité d'une masse résonnante sphérique comme détecteur d'ondes gravitationnelles, diploma thesis, Université de Genève (2005)
- [20] E. Coccia, V. Fafone, G. Frossati, J.A. Lobo and J.A. Ortega, Phys. Rev. D **57**, 2051 (1998).
- [21] M. Bonaldi et al, Phys. Rev. D **74**, 022003 (2006).
- [22] M. Briant et al, Phys. Rev. D **67**, 102005 (2003)
- [23] J. C. Price, Phys. Rev. D **36**, 3555 (1987).
- [24] M. Bassan, Phys. Rev. D **38**, 2327 (1988).
- [25] M. Bassan, Y. Minenkov and R. Simonetti, Proceedings of the Virgo Conference on Gravitational Waves: Sources and Detectors, Cascina, Mar.1996- World Scientific 1997, pag.225-228